

Similitude model experiments for studying slip-buckling failures in high and steep side slopes set along the bedding plane of layered rocks

As the scale of open pit mining and mining intensity have increased continuously over time, the stability of high and steep side slopes have become a key issue that must be addressed in open pit mines. A number of cases have shown that high and steep side slopes with bedded structures are highly susceptible to failure, and these failures may lead to significant damage and destruction. In this work, indoor modelling experiments were performed to study slip-buckling failures in high and steep side slopes set along the bedding plane of layered rocks. Here, experimental similarity criteria were derived according to similarity principles to produce an accurate match with the subject of this study and to select similarity constants. River sand, plaster, and barite were selected as equivalent materials in this experiment, and matching tests were performed. Fuzzy comprehensive evaluation was used to determine the optimal matching scheme on the basis of prototype similarity and physico-mechanical parameters including density, compressive strength, elastic modulus, and Poisson's ratio. The model was filled and constructed through layered filling and tamping, and observation points were installed throughout the model. Based on the subject selected for this study and dynamic excavation processes in mining simulations, we observed deformations of the model that occurred during excavation and the application of a load by a hydraulic servo loading system set on the top of the model. Through analyses of the results, it was found that rocks on the upper part of the slope slipped along the bedding, while slip-buckling failure occurred at the foot of the slope. Finally, the most dangerous

slippage surface was identified as a composite surface with flat and arced surfaces.

Keywords: Side slopes along rock layers, matching of equivalent materials, loading system, similitude model experiment.

1. Introduction

As sedimentary rocks with bedded structures account for 2/3 of the earth's landmass, construction projects are frequently performed in this variety of rock mass; thus, the stability of bedded side slopes is one of the most frequently encountered problems in engineering projects. A number of cases have shown that high and steep side slopes with bedded rock masses are highly prone to failure [1, 2] and are capable of causing significant damage. In-depth studies on the types of failure in bedded side slopes and the mechanisms and deformation characteristics of these failures are thus necessary to ensure the safety and reliability of high and steep bedded side slopes, and the findings derived from these studies are also of significant importance for engineering projects. In this work, an indoor modelling experiment was performed to study slip-buckling failures in high and steep side slopes set along the bedding plane of layered rocks.

2. Similitude matching tests

2.1 SIMILARITY CRITERIA

The high and steep side slopes of an iron mine in Yunnan was chosen as the subject for this study, and dimensional analyses were used to derive the similarity criteria of this experiment.

The parameters that affect the stability of side slopes in open pit mines include [3]: the slope geometric parameter l , density ρ , shear strength indices c and φ , Poisson's ratio μ , modulus of deformation E , gravitational acceleration g , stress σ , strain ε , displacement u , and time t .

Messrs. Yiming Wen, Yong Cheng and You Lin, Mining Engineering Faculty, Kunming Metallurgy College, Kunming 650 033, Wei Liang*, Institute of Mining Engineering, Guizhou Institute of Technology, Guizhou 550 003, Chong Chen, Yunnan ChiHong Zn&Ge Co, Qujing 655 011, Xiaoyan Zeng, Continuous Education College, Kunming Medical University, Kunming 650 031, Wei Sun, Faculty of Land Resource Engineering, Kunming University of Science and Technology, Kunming 650 093, China. E-mail: yimingwen-kmmc@foxmail.com

The relationships between each of these physical properties were expressed using equation (1) in similitude model experiments:

$$f(l, \rho, g, c, E, \mu, \sigma, \varepsilon, u, t) = 0 \quad \dots \quad (1)$$

In this equation, ρ , c , φ , μ , E , g , and l are characteristic parameters taken from the model experiment's design, while σ , ε , and u are derived physical quantities. φ , μ , and ε are dimensionless quantities. l and u have the same dimensions, and c , E , and σ also have the same dimensions.

A dimensional analysis using the [MLT] dimensional system was performed on the parameters of the equation above, from which the following was obtained:

$$[L] = [L]; [\rho] = [M][L]^{-3}; [g] = [L][T]^{-2}; [c] = [M][L]^{-2}[T]^{-2}; [E] = [M][L]^{-2}[T]^{-2}; [\sigma] = [M][L]^{-1}[T]^{-2};$$

The analytic table of the dimensional matrix is shown in Table 1.

Because all dimensionless quantities have a similarity ratio of 1, quantities that have the same dimension then have the same similarity ratio and may be treated as quantities within the same set in this analysis. Therefore, equation (1) has five sets of independent dimensions. By selecting l , ρ , and g as basic physical quantities, three dimensionless π terms may be obtained from equation (1), as well as an equation that is expressed in terms of π .

$$\begin{aligned} f(\pi_1, \pi_2, \pi_3) &= 0 \\ \pi_1 &= \frac{C}{l\rho g} \\ \pi_2 &= \frac{u}{l} \\ \pi_3 &= \frac{t}{l^{1/2}g^{1/2}} \end{aligned} \quad \dots \quad (2)$$

All physical quantities with the same dimensions can be expressed using the same π term, and parameters may be mutually substituted by corresponding quantities with the same dimensions. Therefore, we have:

$$\begin{aligned} \pi_4 &= \frac{E}{l\rho g} \\ \pi_5 &= \frac{\sigma}{l\rho g} \end{aligned} \quad \dots \quad (3)$$

For mutually similar phenomena, the similarity criteria of the prototype and model in the corresponding space, time, and forces are equivalent; therefore, the π relationships between the prototype and model should also be the same. The subscripts p and m denote the prototype and model, respectively, and we thus have:

$$\begin{aligned} \pi_{1m} &= \pi_{1p}; \frac{c_m}{l_m \rho_m g} = \frac{c_p}{l_p \rho_p g} \\ &\vdots \\ \pi_{4m} &= \pi_{4p}; \frac{u_m}{l_m} = \frac{u_p}{l_p} \\ \pi_{5m} &= \pi_{5p}; \frac{t_m}{l_m^{1/2} g^{1/2}} = \frac{t_p}{l_p^{1/2} g^{1/2}} \end{aligned} \quad \dots \quad (4)$$

The first similarity theorem states that if two phenomena are similar, then their similarity index is equal to 1. Hence, $C_\varphi = C_\mu = C_\varepsilon = 1$, and $C_g = 1$, $C_l = n$. The model experiment's similarity criteria were thus obtained as follows:

$$\begin{aligned} C &= C_\mu = C_\varepsilon = 1 \\ C_\sigma &= C_c = C_E = C_{Rt} = C_{Rc} = C_l C_\gamma \\ C_u &= C_l \\ C_t &= \sqrt{C_l} \end{aligned} \quad \dots \quad (5)$$

In this equation, C_φ is the internal friction angle constant, C_μ is the Poisson ratio constant, C_ε is the strain similarity constant, C_σ is the stress similarity constant, C_c is the cohesion similarity constant, C_E is the elastic modulus similarity constant, C_{Rt} is the tensile strength similarity constant, C_{Rc} is the compressive strength similarity constant, C_γ is the density similarity constant, C_u is the displacement similarity constant, C_l is the time similarity constant, and C_t is the geometric similarity constant.

The P30 section was selected for similitude modelling experiments, and the similarity constants are $C_l = 150$, $C_\gamma = 1.5$, $C_\mu = C_\varepsilon = C_\varphi = 1$, and $C_R = C_E = C_\sigma = C_c = 225$.

2.2 EQUIVALENT MATERIAL MATCHING

After conversions were performed based on similarity theory, density, compressive strength, elastic modulus, and Poisson's ratio were selected as the main similarity indices for

TABLE 1: RESULTS OF TABLE OF DIMENSIONAL ANALYSIS

Basic dimension	1	ρ	g	c	φ	E	μ	σ	ε	u	t
M	0	1	0	1	0	1	0	1	0	0	0
L	1	-3	1	-2	0	-2	0	-1	0	1	0
T	0	0	-2	-2	0	-2	0	-2	0	0	1

Notes: The slope geometric parameter l , density ρ , gravitational acceleration g , shear strength indices c and φ , modulus of deformation E , Poisson's ratio μ , stress σ , strain ε , displacement u , and time t

TABLE 2: PHYSICO-MECHANICAL PARAMETERS OF MINERALS

Lithology	Bulk density (g/cm ³)	Compressive strength (KPa)	Elastic modulus (MPa)	Poisson ratio
Skarn	2.17	499.82	11.60	0.213
Marble	1.79	253.33	21.02	0.342
Marbleized limestone	1.77	310.04	19.76	0.287
Limestone	1.79	287.60	15.64	0.207

TABLE 3: OPTIMAL SIMILARITY MATCHING SCHEME

Lithology	Skarn	Marble	Marbleized limestone	Limestone
Matching scheme				
River sand: barite: plaster	9:0.5:1.0	10:1.0:0.5	10:1.0:0.5	10:1.0:0.5

the model and prototype, while river sand, barite, and plaster were selected as simulated matching materials for matching tests [4]. A three-factor-three-level orthogonal test was used in the matching test. By using fuzzy comprehensive evaluation methods to screen the results of the matching test [5], we obtained an optimal similarity matching scheme for skarn, marble, marbleized limestone, and limestone (parameters shown in Table 2), is shown in Table 3.

3. Similitude model experiment

3.1 PROCEDURES OF THE SIMILITUDE MODEL EXPERIMENT

Artificial layered filling methods were used to construct the model for this experiment. The model had a pile height of 120 cm, bedding angle of 55°, and bedding thickness of 1 cm. Fifteen rows of observation points were installed in the model, and the rock formation had a total of 13 layers with 347 points of observation, as shown in Figs.1 and 2.

Each downward excavation was performed 20 cm vertically (which corresponds to a 30-m height on-site), with a bench



Fig.1 Photograph of model

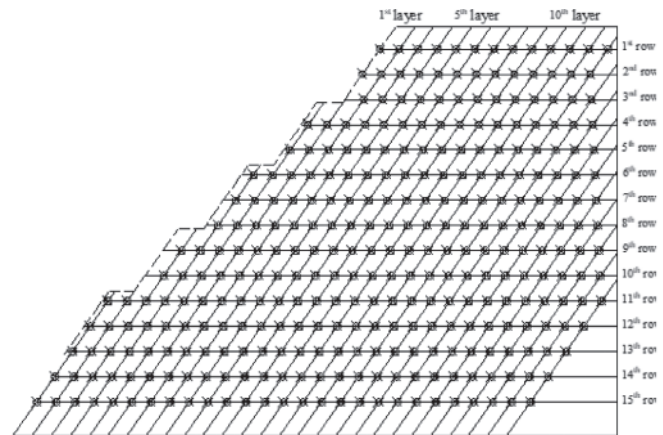


Fig.2 Schematic of layout of observation points

width of 8 cm (corresponding to a 12-m bench width on-site) and a bottom width of 20 cm. Five excavations were performed in total (corresponding to an on-site vertical height of 150 m). After the excavations were completed, a hydraulic servo loading system applied loads to the top of the model (Fig.3), with the loading weight increasing gradually at a rate of 0.05



(a) Fourth excavation of model (corresponding to 120 m on-site)



(b) Third loading of model (corresponding to 450 m on-site)
Fig.3 Photographs of experimental procedures performed on side slope model

t/min. The simulation of high side slopes was thus realized by substituting rock masses on the top of a slope with the application of a load. Sun D L [6] showed that this form of loading was a reasonable substitute for loads on the top of a high side slope. Observations were performed when the model was loaded to 0.28 t, 0.73 t, and 1.35 t. These loads correspond to simulations of side slope heights of 250 m, 350 m, and 450 m, respectively. The deformation of the model at each of these points was observed and recorded. During these observations, a theodolite was used to measure the horizontal and vertical angles at each observation point in order to calculate the positional difference of the observation point from its initial position. From this calculation, the deformation-related displacement of each observation point in the model was calculated. This ultimately gives the state of deformation of the model [7].

3.2 EXPERIMENTAL RESULTS AND ANALYSIS

(1) Side slope deformation displacement vector

The range of influence of the side slope deformations was calculated from the displacements of the observation points. This is shown in Table 4.

As the side slope height of the model gradually increased, it became clear that the patterns and characteristics of the side slope model's deformation during excavation and loading were significantly different. The deformation of the side slope during excavation was relatively low. The directions of the displacement vector mainly indicated downward movement in the bedding, and the range of influence of the deformations was also relatively small. During the loading stage, the

TABLE 4: STATISTICAL TABLE OF RANGE OF INFLUENCE OF SLOPE DEFORMATIONS

Simulated side slope height (m)	30	60	90	120	150	250	350	450
Depth of vertical influence (cm)	24	42	66	84	120	120	120	120
Depth of horizontal influence (cm)	32	40	72	112	144	152	160	176

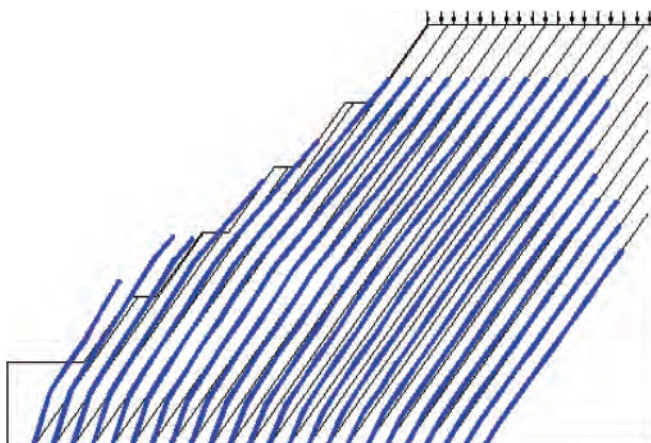


Fig.4 Map of displacement and deformation in bedding following application of third load

direction of the displacement vectors transformed from being pointed away from the slope to an oblique upward direction, which manifested as a partial bulging at the foot of the slope that gradually increased in quantity and range as the loading continued to increase.

(2) Bedding deformation

Buckling deformation occurred in the bedding during excavation and loading, and the buckling length increased gradually as the excavation and loading of the side slope gradually increased. A statistical analysis of the buckling length in the first layer of the side slope model was performed. The relationship between the height of the side slope and the buckling length is shown in Table 5. Bedding deformation may be illustrated by connecting the end points of displacement vectors on the same bedding layer into lines, as shown in Fig.4.

From Fig.5, it may be inferred that the buckling length of the bedding increases non-linearly with increase in the height of the side slope, and reaches its maximum when the side slope height has increased to a certain value. During excavation, the starting points of buckling deformation are

TABLE 5: BUCKLING LENGTH OF BEDDING

Simulated side slope height (m)	120	150	250	350	450
Buckling length (cm)	46	63	91	111	124
Position of the initial segment (cm)	45-91	53-116	55-146	35-146	22-146

close to each other, but the end-point shifts downward as the excavation progresses. During the loading stage, however, the buckling segment no longer extends downward owing to constraints from the bottom of the model. Instead, the upper part of the segment gradually extends upward, thus increasing the deformation length.

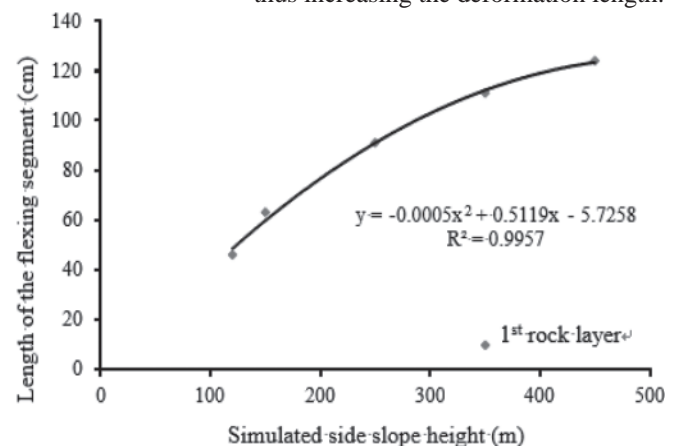


Fig.5 Trend regression chart of buckling length and side slope height

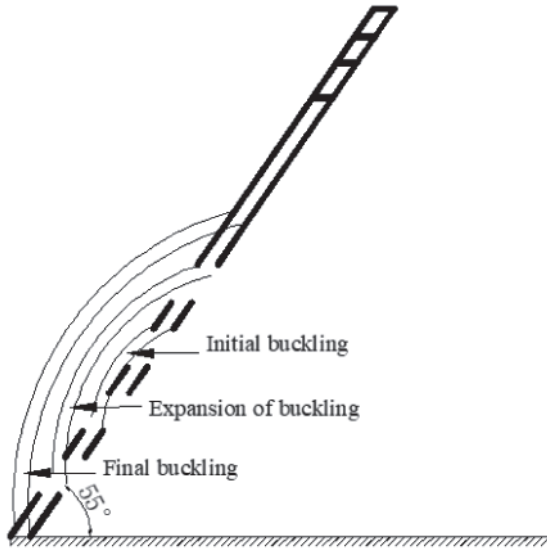


Fig.6 Evolution of buckling deformation in rock layer

The progress of the deformation is consistent with the evolutionary model of buckling deformation in bedded rock masses shown in Fig.6. Buckling deformation in side slopes along the bedding plane was absent during the initial stages of excavation, and compressive deformation is the primary form of bedding deformation during these stages. As the excavation progresses, the bottom of the bedding begins to present buckling deformation as the height of the side slope increases. Further increase in the side slope height leads to large buckling deformations in the bedding, such that the deformations expand from both ends of the initial buckling position.

(3) Patterns of side slope deformation, and the slippage surface with the highest potential for danger

The displacement magnitude of each observation point in each vertical layer can be calculated through their horizontal and vertical displacements. This is equivalent to the rock layer's magnitude of buckling deformation, and is denoted as the buckling deflection. Deflections (of the vertical layer) in the direction of the free surface are positive, while deflections toward the insides of the slope are negative. Fig.7 summarizes the buckling deflections that occur in each of the observation points in the first rock layer, from the excavation stage to the

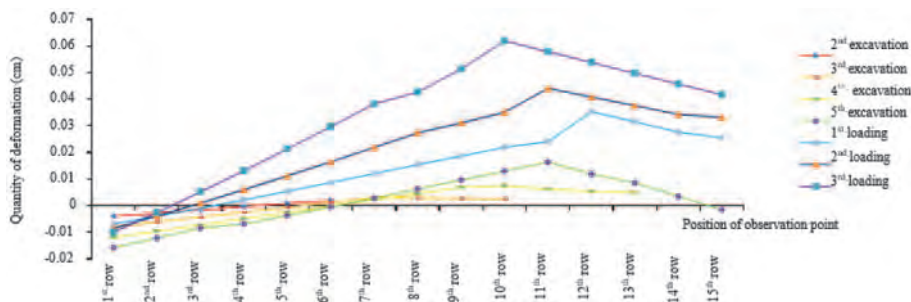


Fig.7 Buckling deflections in first layer

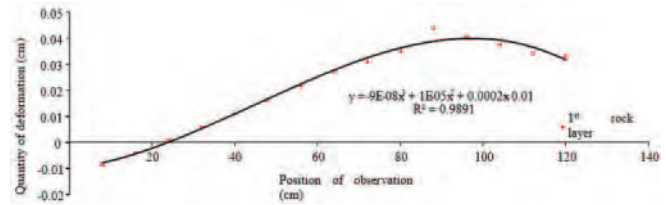


Fig.8 Trend chart of deformation in rock layer

end of the loading stage. This figure characterizes patterns of change in the slope model from the top to the bottom of the rock layer. Using results obtained from the second loading, a trend regression chart of buckling deflections in the first rock layer was created, and the regression equation was also solved, as shown in Fig.8.

In Fig.8, it is shown that the deformation of the upper part of the rock layer is negative and manifests as deformation occurs toward the inside of the slope. After ~25 cm in the downward direction, the deformation of the rock layer becomes positive, and the bulging toward the free surface and deformation gradually decreases as the rock layer develops downward. However, the quantity of the bulging deformation decreases after some point around 100 cm. Buckling deformations of the rock layer can be treated as a plane strain problem. If we neglect the constraints imposed by the ends of the rock layer, then a rock layer may be simplified and treated as a beam of rock. The point of maximum deflection in a rock beam's buckling then corresponds to the point of maximum buckling deformation in a rock layer. By connecting these points with a line, we may then illustrate the potential slippage surface of buckling-deformed positions in the bedding [8]; this slippage surface represents the interface where a sliding mass will slide out of the slope. By combining the inter-layer dislocation boundaries generated by the sliding portion with the deformation curve of the buckling-deformed positions, we then obtain the slippage surface with the highest potential for danger in deformation failures of the side slope model.

From an analysis of Fig.9, it may be inferred that the most dangerous slippage surface is composed of two parts. The first part is a straight line, which presents in the slope as rock layers where inter-layer dislocations have occurred. The second part is a curve, which presents in the slope as a line

that connects positions with the highest level of buckling and bulging deformation in each layer. Hence, the slippage surface with the highest potential for danger in this side slope model experiment is a composite surface with flat and arced surfaces. In addition, the pattern of change in the points of maximum buckling deformation of each rock layer within the slope have been characterized; it

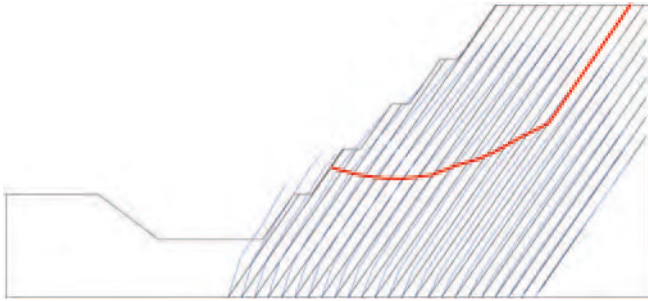


Fig.9 Position of slippage surface with highest potential for danger (loaded to 450 m)

is shown that these points gradually migrate upward as they progress from the slope's free surface toward the inside of the slope, which gradually weakens their degree of influence inside the slope. This is consistent with the presentation of engineering failures that were encountered during actual operations on side slopes. Hence, the similitude model experiment is capable of reflecting the realities of the prototype.

4. Conclusions

In this work, an iron mine in Yunnan was selected as the subject of study, and similitude model experiment criteria were derived according to similarity principles. An indoor simulation experiment was then performed to study slip-buckling failures in high and steep slopes set along the bedding planes of layered rocks through matching physical-mechanical parameters such as density, compressive strength, elastic modulus, and Poisson's ratio with those of the prototype. Through the application of loads on the top of the model, we succeeded in simulating high side slopes using small-scale models, and obtained deformation characteristics and patterns of this type of side slope in different stages. The findings of this work will thus provide an experimental reference for in-depth analyses of failures and damage in high and steep side slopes set along the bedding planes of layered rocks.

Acknowledgments

This work was funded by the project supported by Youth Foundation of Yunnan Province (no. 2013FD059).

References

1. Du, J. (2014): "Study on instability mode of layered slope in Jianshan Phosphate Mine," Kunming University of Science and Technology, pp. 1-153, 2014.
2. Sun, H. F. (2014): "Study on Slope monitoring and forecasting in Jianshan Phosphate Mine," Kunming University of Science and Technology, pp. 1-206, 2014.
3. Zhang, X., Jiang, Q., Chen, N., Wei, W. and Feng, X. (2016): "Laboratory investigation on shear behavior of rock joints and a new peak shear strength criterion," *Rock Mechanics and Rock Engineering*, vol. 49, no.9, pp. 3495-3512, Sep. 2016.
4. Xiao, H. (2014): "Similitude Model Experiments for Studying The excavation process in Stratified rock slopes," Kunming University of Science and Technology, pp. 1-113, 2014.
5. Xu, J. and Li, K. G. (2006): "Application of fuzzy theory on slope stability assesment for expressway," *The Chinese Journal of Geological Hazard and Control*, vol. 17, no. 2, pp. 61-64, 2006.
6. Sun, D. L., Hou, K. P. and Yang, C. L. (2004): "Research on Simplified Stability Calculation of Stepped Slop," *Mining Research and Development*, vol. 25, no. 4, pp. 18-21, 2004.
7. Assefa, S., Graziani, A. and Lembo-Fazio, A. (2016): "A slope movement in a complex rock formation: Deformation measurements and DEM modelling," *Engineering Geology*, vol. 219, pp. 74-91, Mar. 2016.
8. Liu, X. Y. and Yuan, C. M. (2016): "Research on treatment technology of super high slope of weathered rock mass," *Highways & Transportation in Inner Mongolia*, no. 5, pp. 35-37, Dec. 2016. DOI.

JOURNAL OF MINES, METALS & FUELS

Special Issue on

R&D IN CHINESE MINING INDUSTRY

The trends and prospects in China's research and development vis-à-vis mining industry are specifically discussed in the various papers in this special of the journal highlighting new and varied faces of research and development in Chinese mining industry. It also highlights the potential challenges which Chinese policy makers have to face in the coming decades.

China has made considerable progress in science and technology in recent years. In particular China has become a leading investor in research and development (R&D). The Journal of Mines, Metals & Fuels is privileged to present this timely published special issue to highlight new awareness of mineral industry through application of new industrial practice in China.

Price per copy: Rs.500.00; £35.00 or \$55.00

For copies, place your orders with:

The Manager

Books & Journals Private Ltd., 6/2 Madan Street (3rd Floor), Kolkata 700 072

Tel: +91 33 22126526 Fax: +91 33 22126348

E-mail: bnjournals@gmail.com / pradipchanda@yahoo.co.uk

Website: www.journalmp.com / www.jmmf.info